A model perspective on total tropospheric O_3 column variability and implications for satellite observations

A. T. J. de Laat and I. Aben
National Institute for Space Research, Utrecht, Netherlands

G. J. Roelofs
Institute for Marine and Atmospheric Research, Utrecht University, Utrecht, Netherlands

Received 22 July 2004; revised 4 March 2005; accepted 17 March 2005; published 12 July 2005.

[1] In recent years several methods have been developed that derive total tropospheric O_3 columns from satellite measurements. However, one issue that has not been paid much attention to is the interpretation of (extratropical) total tropospheric O_3 columns. Different processes contribute to the total tropospheric O_3 column: stratosphere-troposphere exchange, tropospheric O_3 production and loss, transport and the height of the tropopause. Each process contributes differently to the total tropospheric O_3 column variability depending on season, geographical location, and altitude. This paper investigates the contribution of these different processes on total tropospheric O_3 column variability using a chemistry-climate model simulation of tropospheric O_3, and reflects on the implications for total tropospheric O_3 column measurements. On the basis of tropospheric O_3 column (satellite) measurements and without other sources of information (e.g., model simulations, observations of other trace species) it is not possible to determine the separate contributions by the aforementioned processes to the extratropical total tropospheric O_3 column variability. Furthermore, typical extratropical synoptic-scale (daily) total tropospheric O_3 column variability is of the order of 10 DU (1-σ value), implying the errors in (satellite) measurements should be of the order of magnitude at maximum ($\sim$10 DU) for daily measurements. For tropical total tropospheric O_3 column (satellite) measurements the requirements are less stringent because the most important variability occurs on seasonal timescales. Errors in tropical total tropospheric O_3 column (TTOC) measurements should be of the order of 5 DU for monthly means.

Citation: de Laat, A. T. J., I. Aben, and G. J. Roelofs (2005), A model perspective on total tropospheric O_3 column variability and implications for satellite observations, *J. Geophys. Res.*, *110*, D13303, doi:10.1029/2004JD005264.

1. Introduction

[2] Over the last 2 decades, interest in observing the chemical composition of the atmosphere from space has been increasing. The longest currently available data sets are the satellite measurements of atmospheric O_3 by the Total Ozone Monitoring Satellite (TOMS) and the solar backscatter ultraviolet (SBUV) instruments. These two instruments have been monitoring atmospheric O_3 since the late 1970s from various satellite platforms (TOMS 2003: http://toms.gsfc.nasa.gov/; SBUV2003: http://orbitnet.nesdis.noaa.gov/crad/sit/ozone/). The time series of satellite-measured O_3 are being used to investigate the seasonal, annual, and interannual variability of O_3. Recently several new methods have been developed to derive tropospheric O_3 information from satellite measurements [*Fishman et al.*, 1990; *Hudson and Thompson*, 1998; *Kim et al.*, 1998; *Fishman and Brackett*, 1997; *Ziemke et al.*, 1998; *Fishman and Balok*, 1999; *Kim et al.*, 2001; *Newchurch et al.*, 2003; *Fishman et al.*, 2003; *Valks et al.*, 2003]. All methods retrieve the total tropospheric O_3 column, i.e., the total amount of O_3 between Earth's surface and the tropopause (from here on we will refer to the total tropospheric O_3 column as TTOC, plural as TTOCs). Two topics that have been studied with TTOCs are biomass burning (equatorial Africa and South America) and the role of El Nino–Southern Oscillation (ENSO) on tropospheric O_3 [*Ziemke et al.*, 1996; *Roelofs et al.*, 1997a; *Chandra et al.*, 1998; *Thompson and Hudson*, 1999; *Ziemke and Chandra*, 1999; *Peters et al.*, 2001; *Thompson et al.*, 2001; *Peters et al.*, 2002]. TTOCs outside of the tropics also have been studied, albeit less extensively. Subject areas include the impact and extent of surface pollution emissions on free tropospheric O_3 away from the emission source. Examples are the Asian pollution over the Pacific and North American pollution over the Atlantic [*Fishman and Balok*, 1999; *Fishman et al.*, 2003; *Pierce et al.*, 2003], and the relation between variations in O_3 and circulation patterns such as the North Atlantic Oscillation (NAO) [*Creilson et al.*, 2003].

[3] The different satellite TTOC measurements have uncertainties that are associated with errors in the measured

0148-0227/05/2004JD005264$09.00

spectra, retrieval algorithms, the use of a priori information, and the presence of clouds. Validation consists mainly of comparing monthly mean TTOC column measurements from sonde observations with satellite measured TTOCs. Error estimates of TTOC values for these methods range from 10 to 50% or 5–20 DU for monthly means [*Kim et al.*, 1998; *Ziemke et al.*, 1998; *Fishman and Balok*, 1999; *Kim et al.*, 2001; *Newchurch et al.*, 2001, 2003].

[4] Variability of tropospheric O_3 in the tropics is generally determined by seasonal variations in circulations patterns (for example, monsoons, El Niño) and seasonal variations in O_3 precursor emissions (for example, biomass burning). For a more elaborate description of the processes that control tropospheric O_3, see, for example, *Brasseur et al.* [1999]. Stratosphere-troposphere exchange (from here on referred to as STE) is of minor importance for the tropical O_3 budget [e.g., *Lelieveld and Dentener*, 2000; *Kentarchos and Roelofs*, 2003]. Furthermore, because major variations in tropical TTOCs occur on monthly timescales and the tropopause height varies little in the tropics, monthly mean tropical TTOCs are very useful for studying tropical O_3 variability and are straightforward to interpret.

[5] Outside of the tropics, seasonal tropospheric O_3 variability is determined by both tropospheric O_3 production/loss and STE [*Lelieveld and Dentener*, 2000]. Furthermore, because the highest tropospheric O_3 concentrations are found close the tropopause, variations in the tropopause height also have an impact on TTOC values. The 1-σ variability of the tropospheric air column thickness is about 10–15% (root-mean-square; see later in Figure 9), which is a rough estimate for the TTOC variability related to tropopause height variations. The variations in extratropical tropospheric O_3 columns reflect the complex interaction of photochemical O_3 production and atmospheric dynamics (STE and the thickness of the troposphere). Since none of these parameters can be measured directly by satellite instruments, it is likely that interpretation of extratropical TTOCs will only be possible with the use of additional information sources (other measured species, model analyses, etc.).

[6] This paper investigates and highlights the role of the different processes on TTOC variability using the ECHAM chemistry-climate model. Different tracers for total O_3 and O_3 from stratospheric origin are used to estimate the separate contributions to TTOC variability by STE and by photochemical ozone formation in the troposphere. It is investigated which part of the TTOC can be attributed to stratospheric and tropospheric O_3 production or by changes in the thickness of the tropospheric air column. Note that it is beyond the scope of this paper to investigate the origin of tropospheric O_3 at a particular location.

[7] A significant part of tropospheric O_3 variability is caused by processes that occur on short (daily) timescales. Without understanding the short-time variability it is difficult to understand longer timescale variability. In addition, satellite TTOC measurements are often provided as monthly means, but these are, in turn, determined by TTOC variability on shorter timescales. We decided in this study to focus on shortest timescales of important variability, i.e., synoptic and seasonal, for which a 1-year simulation of tropospheric O_3 is sufficient. The analysis presented here will also be used to reflect on what is required for (satellite) measurements in order to measure tropospheric O_3 variability, which means that the accuracy and time/space resolution of the measurements is such that the important TTOC variability is captured by the measurements. In addition, it should be noted that the requirements that are defined in this paper apply for any measurement error that cannot be corrected for, either random or systematic (systematic errors often cannot be characterized sufficiently to determine a correction).

[8] The paper is structured as follows: Section 2 describes the ECHAM model and presents a brief comparison between modeled and measured TTOCs. In section 3 the global variability of modeled TTOCs and the roles of tropospheric O_3 production and STE are investigated. Section 4 analyzes the TTOC variability at several individual model grid points in terms of the contributions of O_3 above and below 10 km altitude (the influence of tropopause height variations on TTOC variability) as well as below 10 and 2 km altitude. In section 5 the relation between TTOCs and tropospheric O_3 production, STE, and tropopause heights is quantified. Section 6 discusses the consequences of the analysis presented in this paper for the accuracy of satellite measurements of TTOCs. A short summary and conclusions follow in section 7.

2. The ECHAM Model

2.1. Model Description

[9] The general circulation model (GCM) used for this study is the 19-layer European Center Hamburg Model (ECHAM), version 4. A model simulation was performed at T63-resolution, approximately $1.9° \times 1.9°$ with a time resolution of 900 s. The model uses a hybrid σ-ρ vertical coordinate system from the surface to 10 hPa. Average pressure levels are 990, 970, 950, 900, 840, 760, 670, 580, 490, 400, 320, 250, 190, 140, 100, 70, 50, 30, and 10 hPa. Corresponding approximate midlayer altitudes are 0.03, 0.14, 0.38, 0.78, 1.4, 2.1, 3.1, 4.2, 5.6, 7.0, 8.6, 10.2, 11.9, 13.8, 15.9, 18.0, 20.5, 23.8, and 31 km. Tracer transport is calculated using a semi-Lagrangian advection scheme [*Rasch and Williamson*, 1990]. A detailed description of ECHAM version 4 is given by *Roeckner et al.* [1996, 1999].

[10] The model version uses a tropospheric chemistry scheme including emissions of NO, CO, and nonmethane hydrocarbons (NMHC), dry deposition of O_3, NO_2, HNO_3, and H_2O_2, wet deposition of HNO_3 and H_2O_2, parameterized surface CH_4 concentrations, and the Carbon Bond Mechanism 4 (CBM-4) scheme [*Gery et al.*, 1989; *Houweling et al.*, 1998] to describe the nonmethane hydrocarbon (NMHC) chemistry. For a detailed description, see *Roelofs et al.* [1997b], *Kentarchos et al.* [2000], and *Roelofs and Lelieveld* [2000a].

[11] The model does not include a chemical reaction scheme for stratospheric O_3 chemistry. Middle stratospheric ozone is parameterized according to results from a two-dimensional (2-D) troposphere chemistry model [*Brühl and Crutzen*, 1988]. Lower stratospheric O_3 variability is parameterized by using an ozone potential-vorticity correlation [*Roelofs and Lelieveld*, 2000b]. This parameterization is only applied in the extratropical lower stratosphere at latitudes higher than 25°. O_3 is not parameterized between one and two model layers above the tropopause to allow for

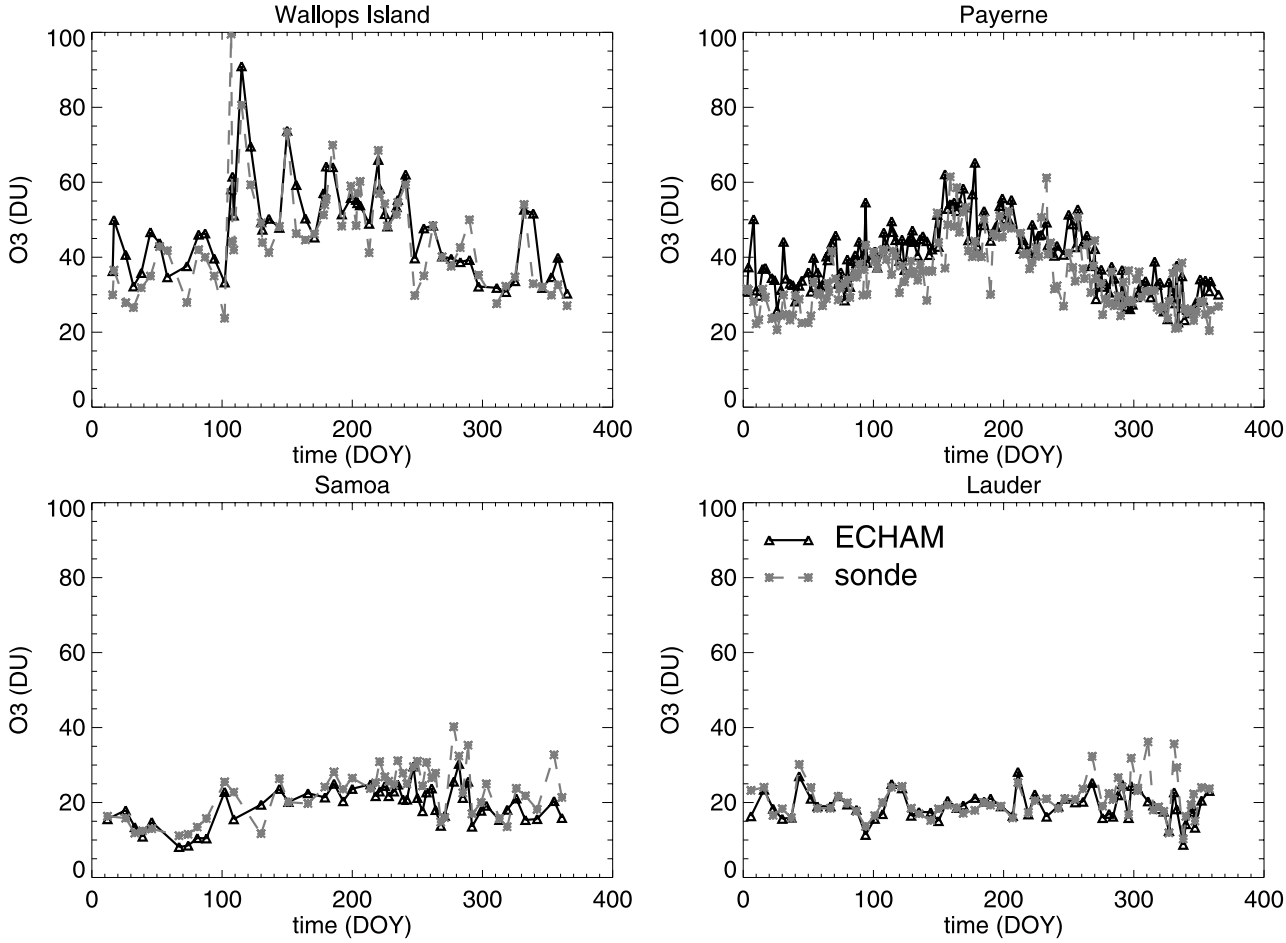

Figure 1. Comparison of measured and modeled TTOCs for 1996 for four different stations: Wallops Island (75.5°W, 37.9°N); Payerne (6.6°E, 46.5°N); Samoa (170.6°W, 14.2°S); and Lauder (169.7°E, 45°S). The solid curve is the model calculated TTOC, the shaded curve is the measured TTOC. Data are obtained from the World Ozone and Ultraviolet radiation Data Centre (WOUDC).

mixing between the upper troposphere and lower stratosphere. The seasonality of lower stratospheric O_3 is well reproduced by this parameterization [*Roelofs and Lelieveld*, 1997; *Kentarchos et al.*, 2000].

[12] Transport of O_3 across the tropopause depends directly on the air motions simulated by the GCM. The simulated tropopause is marked by a potential vorticity of 3.5 10^{-6} K m^2 kg^{-1} s^{-2} poleward of 20°latitude [*Hoerling et al.*, 1993] and by a -2 K km^{-1} temperature lapse rate equatorward of 20° latitude. In addition, for calculating the TTOC the simulated tropopause was defined at full model levels. Apart from O_3, the model considers a tracer for O_3 that originates from the stratosphere. Modeled O_3 of stratospheric origin will be referred to as "O_3str," and modeled O_3 from tropospheric O_3 production (e.g., O_3 minus O_3str) will be referred to as "O_3trop". The O_3str tracer is treated similar to O_3, with the exception that no tropospheric production occurs. Thus, in the troposphere, O_3str is only destroyed (reactions with OH and HO_2, photodissociation, and surface deposition). The O_3str tracer can be considered as a good first-order proxy for the influence of STE on the modeled tropospheric O_3 budget.

[13] In this study the so-called 'nudging' technique (using European Centre for Medium-Range Weather Forecasts (ECMWF) analyses to simulate the actual meteorology) was applied for the model simulation to enable a direct comparison of modeled trace gases (O_3) with observations. This method is described more extensively by *Jeuken et al.* [1996]. The nudging method has been used for several other studies [*Kentarchos and Roelofs*, 2003; *de Laat*, 2002, and references therein]. For this study the year 1996 was chosen, which was simulated with a resolution of 1.9° × 1.9° (T63). The simulated O_3 distributions resulting from this model simulation have been analyzed and validated extensively in previous studies [*Kentarchos et al.*, 2000, 2001; *Roelofs et al.*, 2003; *Cristofanelli et al.*, 2003; *Meloen et al.*, 2003], although not in terms of TTOC.

[14] The model simulated O_3 seasonality at the surface, in the free troposphere, and in the tropopause region agree well with observations [e.g., *Roelofs and Lelieveld*, 1997, 2000a]. Short-term simulated O_3 variability, e.g., associated with synoptical disturbances, also agrees well with observations [*Kentarchos et al.*, 2000; *Roelofs et al.*, 2003]. Cross-tropopause mass fluxes are in reasonable agreement with observations [*Roelofs et al.*, 1997a, 1997b; *Roelofs and Lelieveld*, 2000b]. However, the relatively coarse vertical resolution near the tropopause and the rather diffusive semi-Lagrangian transport scheme result in an overestimation of the down-

Table 1. Comparison of Modeled and Measured TTOC Values for a Number of O_3 Sonde Stations for 1996[a]

Station	Name	Number of Measurements	Longitude, deg	Latitude, deg	Correlation	Modeled TTOC, DU	Measured TTOC, DU	Difference, DU	Difference, %	RMS Modeled, DU	RMS Measured, DU	RMS Differences, DU
stn014	Tateno	47	140.1	36.0	0.78	43.3	38.3	5.0	13	14.7	15.3	−0.6
stn012	Saporo	30	141.3	43.0	0.92	41.9	38.6	3.3	9	12.9	14.2	−1.3
stn107	**Wallops Island**	**60**	**−75.5**	**37.9**	**0.81**	**48.3**	**45.3**	**3.0**	**7**	**12.0**	**14.4**	**−2.4**
stn221	Legionowo	69	21.0	52.4	0.72	44.5	34.3	10.2	30	11.1	8.1	3.0
stn262	Sodankyla	63	26.6	67.4	0.79	38.6	30.7	7.9	26	10.5	6.5	4.0
stn316	De Bilt	51	5.2	52.1	0.67	43.1	32.9	10.2	31	9.7	10.8	−1.1
stn024	Resolute	22	−95.0	74.7	(0.50)	34.2	28.5	5.7	20	9.4	8.2	0.8
stn007	Kagoshima	32	130.6	31.6	0.86	39.7	38.7	1.0	3	9.2	11.3	−1.1
stn077	Churchill	42	−94.1	58.8	(0.39)	38.4	31.9	6.5	20	9.2	9.3	−0.1
stn099	Hohenpeissenberg.	122	11.0	47.8	0.77	37.6	35.0	2.6	7	9.1	9.4	−0.3
stn156	**Payerne**	**155**	**6.6**	**46.5**	**0.78**	**39.5**	**34.8**	**4.7**	**13**	**8.8**	**8.7**	**0.1**
stn018	Alert	44	−62.3	82.5	0.62	35.1	30.7	4.4	14	8.5	6.6	1.9
stn043	Lerwick	66	−1.2	60.1	0.64	41.2	31.8	9.4	29	7.7	7.1	0.6
stn076	Goose Bay	37	−60.3	53.3	0.67	36.6	31.0	5.6	18	7.0	6.8	0.2
stn021	Edmonton	47	−114.1	53.5	0.78	31.7	28.3	3.4	12	6.5	5.7	0.8
stn315	Eureka	76	−86.4	80.0	(0.46)	31.9	30.5	1.4	5	6.3	8.7	−2.4
stn191	**Samoa**	**50**	**−170.6**	**−14.2**	**0.81**	**19.4**	**22.6**	**−3.2**	**−14**	**5.1**	**7.0**	**1.9**
stn256	**Lauder**	**61**	**169.7**	**−45.0**	**0.71**	**19.1**	**20.8**	**−1.7**	**−8**	**3.8**	**5.2**	**−1.4**
stn441	Easter Island	35	−109.4	−27.2	(0.37)	24.4	27.7	−3.3	−12	3.8	5.1	−1.3

[a]The measurements shown in Figure 1 are indicated in bold. Correlations with values below 0.6 are in parentheses. The table consists of (left to right) station number (from the WOUDC Web site), station name, number of O_3 sonde measurements, longitude, latitude, correlation, mean modeled and measured TTOC, difference between mean measured and modeled TTOC (absolute and relative values), RMS value of modeled and measured TTOCs, and differences between modeled and measured TTOCs.

ward transport of O_3 deeper into the troposphere [*Roelofs et al.*, 2003; *Cristofanelli et al.*, 2003; *Meloen et al.*, 2003].

[15] On annual and global scales the simulated cross-tropopause (459 Tg O_3 yr^{-1}) flux compares well with other estimates: 500–600 Tg O_3 yr^{-1} for MATCH-MPIC [*von Kuhlman*, 2001]; 565 Tg O_3 yr^{-1} for TM3 [*Lelieveld and Dentener*, 2000].

2.2. Validation of Modeled Tropospheric O_3 and TTOCs

[16] Figure 1 shows a comparison of modeled and measured TTOCs for four stations: Payerne, Wallops Island, Samoa, and Lauder (see also Table 1). The measurements were obtained from the World Ozone and Ultraviolet Radiation Data Centre (WOUDC) Web site (http://www.woudc.org). The tropopause heights used to derive the observed TTOC are taken from the model as described in section 2.1 (an estimate of uncertainties associated with the tropopause heights and vertical resolution follows at the end of this section). The model reproduces both seasonal and short-time variations as measured for these stations. A significant positive model bias is found for Payerne, but modeled and measured variability agree quite well. Table 1 summarizes the results for these and other stations. For all northern midlatititude stations, modeled TTOCs are larger than measured TTOCs, especially for the northern European stations (De Bilt, Legionowo, Lerwick, and Sodankyla) as well as for the Canadian stations (Resolute, Churchill, Alert, Goose Bay, and Edmonton). On the other hand, the correlations for the European stations are high (0.6–0.9) and measured and modeled variability agree well (root-mean-square (RMS) values). Furthermore, the model captures geographical variations in mean TTOCs and variability (rms), which are both high in the Northern Hemisphere (NH) and low in the Southern Hemisphere (SH). The model bias in TTOC over Europe agrees with the findings from a model intercomparison [*Cristofanelli et al.*, 2003; *Meloen et al.*, 2003; *Roelofs et al.*, 2003], which attributed the bias to too efficient diffusion of stratospheric O_3 through the model tropopause during synoptical events.

[17] Another potential source of uncertainty is the relatively low vertical model resolution near the tropopause, which is 1–2 km. Modeled tropopause height variability is larger than the vertical model resolution on both short and long timescales (annual rms values are 1–2.5 km, indicating a typical tropopause height variability of 2–5 km). Therefore the model should represent most of the larger tropopause height variations, which affect TTOC variability the most. Note that within the tropics the tropopause height is relatively constant. The sensitivity of the model results to the tropopause location either at full model levels or interpolated between model levels was also investigated (a quadratic interpolation of the temperature profile between grid points to determine the vertical level of the 2 K km^{-1} gradient was used). Typical RMS differences in TTOC values for these two different tropopause height calculations were 0.1–0.2 DU within the tropics, 0.75–1.5 DU in the Southern Hemisphere, and 1.5–2 DU in the Northern Hemisphere. Typical TTOC variability (RMS) ranges from a few DU at clean tropical locations to more than 10 DU at Northern Hemispheric midlatitudes (Table 1). Comparing these numbers shows that the model results are not very

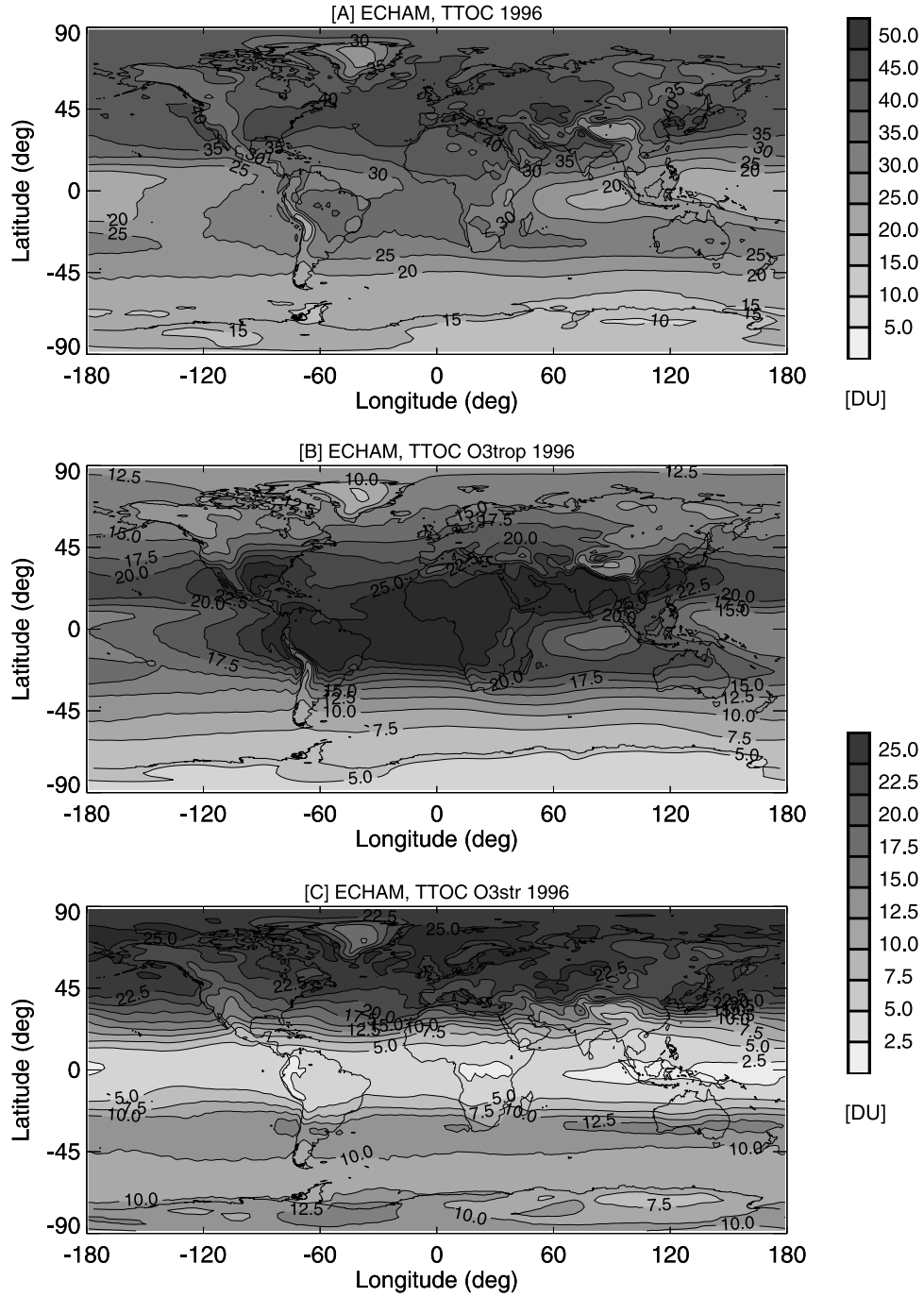

Figure 2. Annual (1996) average total tropospheric O_3 column density (Dobson units, or DU) for (a) O_3, (b) tropospheric O_3 production, and (c) O_3 of stratospheric origin. See color version of this figure at back of this issue.

dependent on the exact tropopause height definition. In section 4 the influence of tropopause height variability on TTOC variability is further investigated.

3. Mean Modeled Global Total Tropospheric O_3 Columns

[18] Figure 2 shows the modeled TTOC values for O_3, O_3trop, and O_3str, averaged over 1 year. TTOC values are higher in the Northern Hemisphere compared with the Southern Hemisphere. Figures 2b and 2c show that this is related to both more tropospheric O_3 production in the Northern Hemisphere (more emissions of O_3 precursors) as well as more STE. Enhanced STE is related to the presence of larger temperature gradients due to more landmasses in the Northern Hemisphere, which causes extratropical cyclones to be more active [*Holton et al.*, 1995], as well as the presence of orography that interacts with the atmospheric circulation [*Wernli and Bourqui*, 2002]. Figure 2b also shows that the O_3trop amount in the tropics

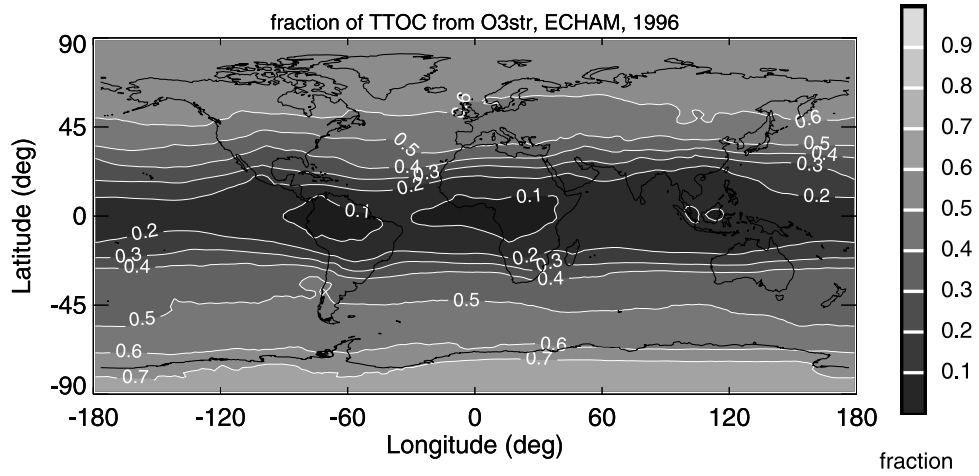

Figure 3. Annual (1996) average fraction of ECHAM modeled total tropospheric O_3 columns attributed to O_3 of stratospheric origin. The residual of this value (that is one minus this values) denotes the contribution of O_3 of tropospheric origin. See color version of this figure at back of this issue.

is larger than at midlatitudes. The tropospheric column is thicker in the tropics and photochemical O_3 production is stronger due to more solar radiation, while the influence of STE is less important. Tropical O_3 production mainly occurs over equatorial America and Africa, at the surface where large amounts of O_3 precursors are emitted (biomass burning) and in the free troposphere from lightning and oxidation of hydrocarbons that have been vertically mixed [e.g., *Lelieveld and Dentener*, 2000]. At the same time, over the equatorial Indian and Pacific oceans, TTOC values are low due to strong vertical mixing of O_3-depleted marine boundary layer air. At ~30°N/S, plumes of tropical O_3trop are advected along the subtropical jets round the globe [e.g., *Thompson et al.*, 1996; *de Laat*, 2002] (the subtropical jet is typically located between 10 and 15 km altitude). Outside of the tropics, tropospheric O_3 production decreases with increasing latitude.

[19] Figure 3 shows the fractional contribution of O_3str (and thus also O_3trop) to the TTOC, averaged for 1996. In the tropics (30°S–30°N) the O_3trop contribution dominates, with the highest contribution close to O_3 precursor emissions (equatorial Africa, South America, and Southeast Asia). A strong gradient in the fractional contributions can be seen around 30°S and 30°N, the location of the subtropical jets, which can be considered as a transition zone between tropics and midlatitudes. Farther poleward the fractional contribution of O_3str increases and of O_3trop decreases because of enhanced STE and reduced tropospheric O_3 production. In the Northern Hemisphere the fractional contribution of O_3trop remains more or less constant around 40% at polar latitudes, mainly because of tropospheric O_3 production that result from O_3 precursor emissions in the Northern Hemisphere. In the Southern Hemisphere, less O_3 precursors are emitted, and therefore the fractional contribution of O_3trop decreases to less than 30% at Southern Hemispheric polar latitudes.

[20] Figure 4 shows the seasonal variations of the modeled zonal mean TTOCs. A separation can be made between the Northern Hemisphere (>30°N), the tropics (30°N–30°S), and the Southern Hemisphere (<30°S). The TTOCs in the

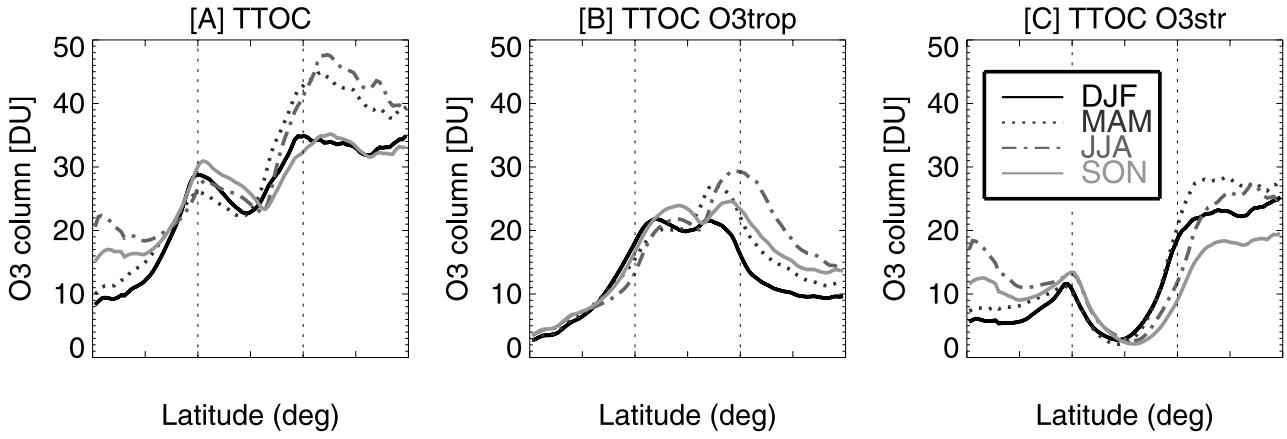

Figure 4. The zonal averaged total tropospheric O_3 column (DU) as a function of season (purple solid curve, DJF; dotted blue curve, MAM; dash-dotted green curve, JJA; dash-dotted red curve, SON). Indicated are (a) the total tropospheric O_3 column, (b) the O_3trop, and (c) O_3str contribution to the total tropospheric O_3 column. See color version of this figure at back of this issue.

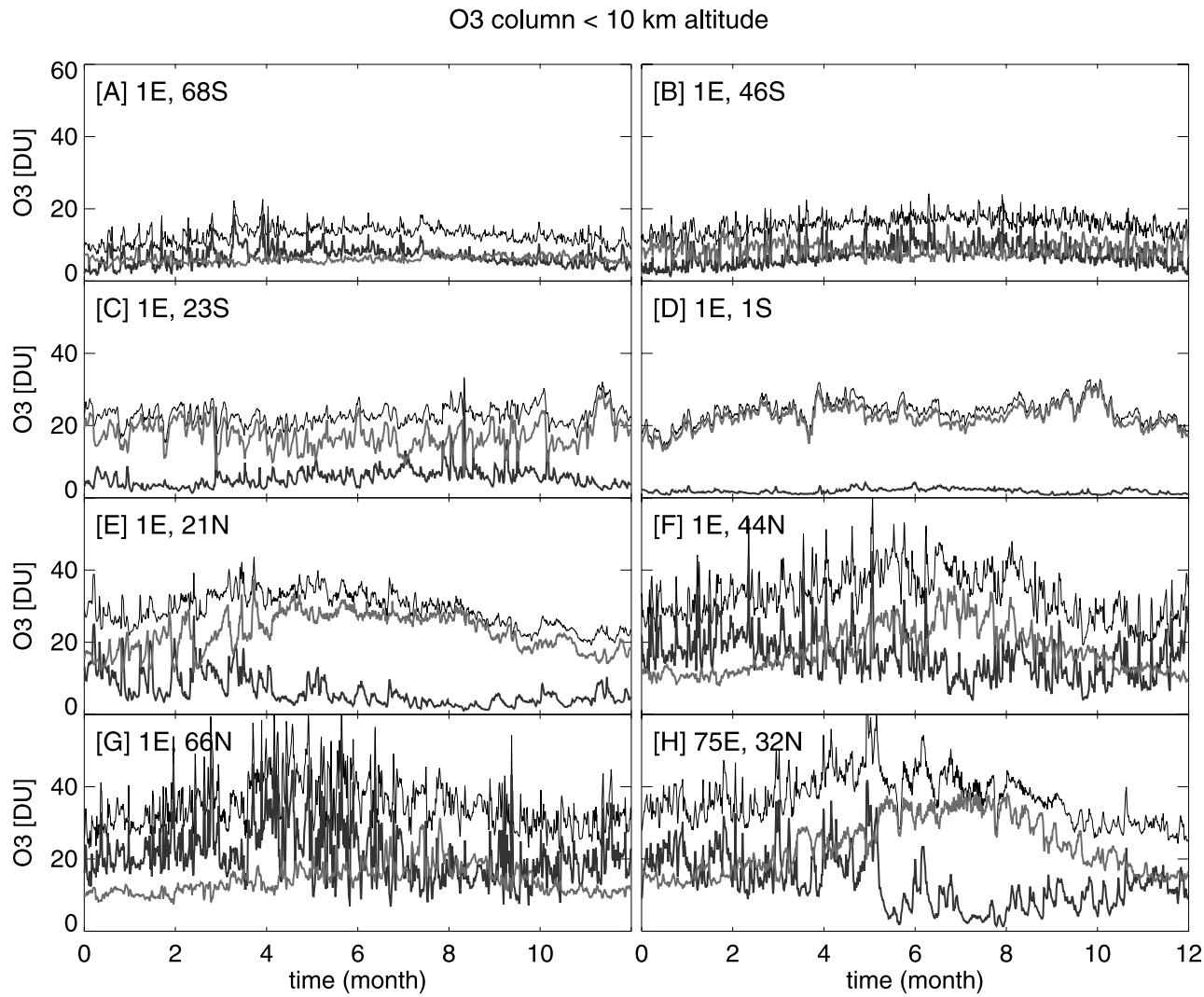

Figure 5. Total O_3 columns (black curve) between the surface and 10-km altitude and the respective O_3trop (red curve) and O_3str (blue curve) partitioning at seven latitudes along 1°E from (a–g) 68°S to 66°N and (h) at 32°N–75°E for the year 1996. The total O_3 column between the surface and 10-km altitude is not affected by tropopause height variations. See color version of this figure at back of this issue.

Northern Hemisphere are largest during spring/summer and smallest during autumn/winter. The Northern Hemispheric O_3trop contribution is largest during summer (June–July–August (JJA)) and smallest during winter (December–January–February (DJF)), following the maximum and minimum in the amount of sunlight (Figure 4b). The seasonal cycle of O_3str in the Northern Hemisphere is different from that of O_3trop, with a maximum during spring (March–April–May (MAM)) and a minimum during autumn (September–October–November (SON)) [see also *Roelofs and Lelieveld*, 1997] (Figure 4c). Stratospheric O_3 amounts are largest during spring and smallest during autumn, because temperature differences between continents-oceans and equator-poles are largest during winter, favoring extratropical cyclone formation that drives STE. In addition, the presence of mountainous regions in the Northern Hemisphere enhances the differences in STE between the hemispheres.

[21] In the tropics, O_3 is mainly determined by O_3trop (Figure 4b). Variations between the seasons are smaller, with a maximum during SON, related to the biomass burning maximum over the equatorial Atlantic Ocean. Along the subtropical jet (30°N) the O_3str contribution increases strongly (Figure 4c), especially in the Northern Hemisphere during winter/spring (DJF/MAM).

[22] In the extratropical Southern Hemisphere, O_3trop is almost independent of season. It can be considered as an O_3-destructive environment due to the absence of O_3 precursor sources in this region. Most O_3trop has to be advected from (sub-) tropical regions and thus its contribution decreases farther away from the tropics. The O_3str contribution is largest during local winter (JJA) and smallest during local summer (DJF).

4. Modeled TTOCs for Individual Grid Points

[23] The analysis presented in Figures 2–4 only considers the globally and seasonally averaged spatial variations in modeled TTOC values. In this section, TTOC variations on shorter timescales are investigated by analyzing modeled

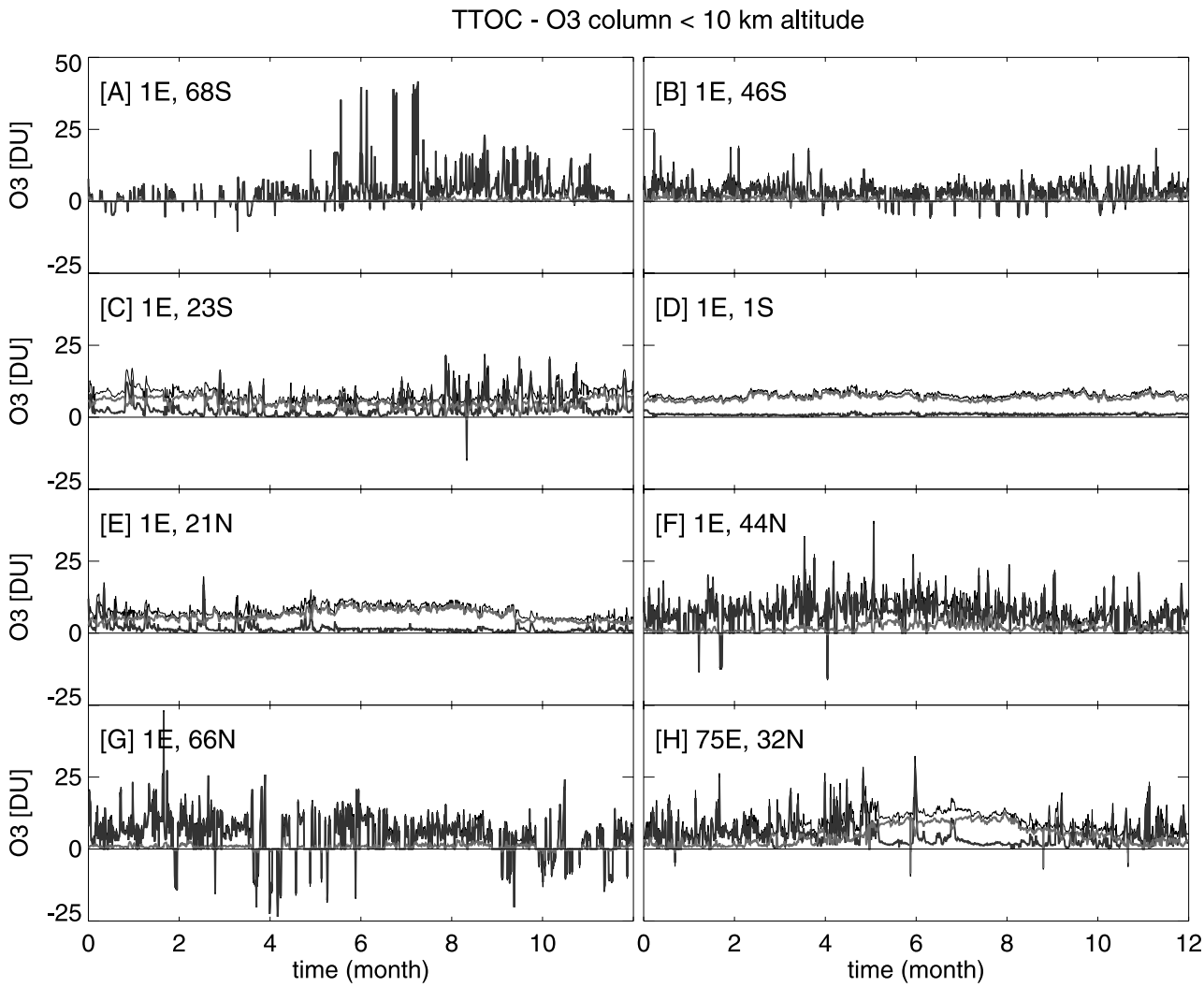

Figure 6. Same as Figure 5 but for the difference between the total tropospheric O_3 column density and the O_3 column between the surface and 10-km altitude. See color version of this figure at back of this issue.

TTOCs for individual model grid points. The purpose is to illustrate TTOC variability on shorter timescales, the influence of tropopause height variations on TTOC variability, and the role of the lower troposphere in TTOC variations. Seven latitudes were selected along 1°E from 68°S to 66°N (Figures 5a–5g). The choice for the 1°E longitude is arbitrary. However, Figure 2 shows that zonal variations are less important than latitudinal variations. The selected locations are to first order representative of the zonal band in which they are located (high/low midlatitudes, transition zone from midlatitude to the tropics and the tropics). In addition, model results are also shown for 32°N–75°E (Figure 5h), which is over the Indian subcontinent just south of the Himalayas. This last example illustrates the complications that can occur in the interpretation of TTOC variability at certain locations.

4.1. Modeled Tropospheric O_3 Column Below 10-km Altitude

[24] First, the temporal variability of TTOC and the O_3trop-O_3str partitioning for O_3 column values below 10-km altitude is investigated, which is not affected by tropopause height variations. In the Southern Hemisphere (68°S, 46°S), the TTOC is small with STE contributing to most of the variability (more for 68°S than 46°S). Furthermore, seasonal variations in the O_3trop contribution are small. At 23°S (subtropics) the partitioning changes, with the largest contribution originating from O_3trop. Although the O_3str contribution is smaller, O_3str still contributes to TTOC variability. At the equator (1°S) all variability is caused by O_3trop, while little O_3str is found. At 21°N (similar to 23°S) most of the O_3 is still of tropospheric origin, although O_3str variability is high during local winter and spring. At 44°N the relative contributions of O_3trop and O_3str are comparable. However, STE is larger during winter than during summer. The O_3trop contribution is more important during summer, caused by more active photochemistry and strong O_3 precursor emissions in the Northern Hemisphere. TTOC variability at 66°N is similar to that at 44°N, albeit that the contribution of O_3trop is smaller due to reduced photochemistry. Note that especially at Northern Hemispheric midlatitudes, variability is high at timescales of days, related to the passage of synoptic systems.

Table 2. Statistics of Modeled O_3 Columns During 1996 for the Same Grid Points as Shown in Figures 5 and 6[a]

	TTOC	TTOC < 2 km	Fraction	σ_1	σ_2
66°S	14.0	2.4	0.17	6.6	0.58
46°S	16.8	2.8	0.17	4.0	0.65
23°S	27.4	3.8	0.14	3.9	0.78
1°S	27.5	4.4	0.16	3.9	0.93
21°N	30.4	6.6	0.22	6.2	1.33
44°N	34.0	7.5	0.22	9.6	1.98
66°N	33.9	6.4	0.19	9.1	1.18
32°N	37.0	9.2	0.25	9.6	1.71

[a]The three leftmost columns show the mean TTOC, the O_3 column below 2-km altitude, and the fraction of the TTOC column located below 2 km altitude. The fourth column (σ_1) is the standard deviation of the TTOC (see also Table 1), and the fifth column (σ_2) is the standard deviation of the O_3 column below 2-km altitude.

[25] Figure 5h shows the northern India location (32°N–75°E). During winter O_3trop and O_3str contribute approximately the same amount to the TTOC, resembling a midlatitude location. During summer (monsoon; wet season) most of the O_3 is tropospheric, with a much smaller contribution of O_3str, resembling a (sub-) tropical location. At the same time, O_3str variability is still large during local summer. Furthermore, the contributions of O_3str and O_3trop to the TTOC variability are weakly anticorrelated, which is related to passage of troughs and ridges along the subtropical jet. Troughs are associated with STE, while ridges cause advection of tropical upper tropospheric African pollution to be advected toward northern India [*de Laat*, 2002].

4.2. Modeled Tropospheric O_3 Column Between 10-km Altitude and the Tropopause

[26] To investigate the influence of tropopause height on TTOC variability the tropospheric O_3 column variability above 10 km is shown in Figure 6. At Southern Hemispheric midlatitudes (Figures 6a and 6b; 68°S and 46°S) as well as Northern Hemispheric midlatitudes (Figures 6f and 6g; 44°N and 66°N) a considerable amount of, and variability in, O_3 occurs between 10-km altitude and the tropopause due to tropopause height variations. This variability is almost entirely caused by O_3str. On occasion the tropopause is also found below 10-km altitude, causing negative differences. The contribution of O_3trop is small above 10-km altitude. For the subtropics (Figures 6c and 6e; 23°S, 21°N) most of the O_3 between 10-km altitude and the tropopause is O_3trop, but most variability is caused by O_3str. Within the tropics (Figure 6d) only a small amount of O_3str is located between 10-km altitude and the tropopause, and tropopause heights vary little. As a result, little variation in the tropospheric O_3 column above 10-km altitude is seen. For northern India (Figure 6g; 32°N–75°E), two distinct periods can be discerned. During autumn–winter–spring most of the O_3 between 10 km and the tropopause is of stratospheric origin, causing a considerable amount of variability, typical for a midlatitude location. During summer the stratospheric contribution reduces considerably and variability is small, while most of the O_3 is O_3trop, typical for a tropical location.

4.3. Modeled Tropospheric O_3 Column Below 2-km Altitude

[27] An important motivation for measuring tropospheric O_3 from space has been the expected future increase in near-surface (atmospheric boundary layer, or ABL) O_3 concentrations, which can be harmful for plants and animals. However, the question can be asked, How much of the TTOC amount and variability is caused by ABL O_3? Table 2 shows the amount and variability of O_3 below 2 km. Comparison with the total O_3 column amount and variability for the eight locations used in Figures 5 and 6 and Table 1 yields an indication of the contribution of ABL O_3. The contribution of O_3 below 2 km varies between 14 and 25% of the TTOC amount. The variability of the O_3 column below 2-km altitude (0.6–2 DU) is likewise considerably smaller than the TTOC variability (3.9–9.6 DU). Thus it can be deduced from this comparison that free tropospheric ozone dominates the TTOC variability, and therefore variations in TTOC are probably not indicative of near-surface O_3 variability.

[28] The fact that only a small fraction the TTOC that is located in the ABL does not exclude the possibility of a relation between variations in TTOC and surface O_3 [see, e.g., *Fishman et al.*, 2003]. At midlatitudes, near-surface O_3 pollution episodes often occur under stagnant high-pressure situations. Increased solar radiation due to reduced cloud cover in such a situation favors photochemical O_3 production throughout the troposphere, resulting in simultaneous increases in near-surface and free tropospheric O_3. The increase in TTOC values may be further enhanced by an increase in the tropopause height. This could give rise to an apparent correlation between near-surface O_3 and TTOC variations, especially during summer.

5. Correlations Between O_3str, O_3trop, and Tropopause Height

[29] In the previous section it was shown that the contribution of O_3str and O_3trop very much depends on geographical location, on season, and on tropopause height. The global relations between these factors are further analyzed using correlation coefficients (linear Pearson correlation coefficient) between the TTOCs (including tropopause height variations) and its stratospheric/tropospheric part (Figure 7a/Figure 7b) for the year 1996. Within the tropics (20°N–20°S), TTOC variability is determined by O_3trop (Figure 7b). Outside of these regions, a positive correlation exists between the TTOC and O_3trop, especially around 45°N–45°S, but the correlations are lower than within the tropics. Note that in the Northern Hemisphere the highest correlations occur over land, related to the emissions of O_3 precursors, which predominantly occur over land. Over the oceans the correlation between the TTOC and O_3trop is small. The Southern Hemisphere shows a similar picture. A correlation exists in a zonal band around 45°S, which is related to the transport of O_3-rich subtropical air from South America and Africa associated with biomass burning [*Thompson et al.*, 1996]. A similar process occurs along the Northern Hemispheric subtropical jet associated with fossil fuel consumption [*de Laat*, 2002].

[30] Figure 7a shows O_3str and TTOC variations correlate strongly outside of the tropics. However, it can also be seen that on occasion a strong correlation exists between O_3 and O_3str columns within the tropics, even though it was shown (Figure 3) that in the tropics the fractional contribution of O_3str is small. These high correlations are related to

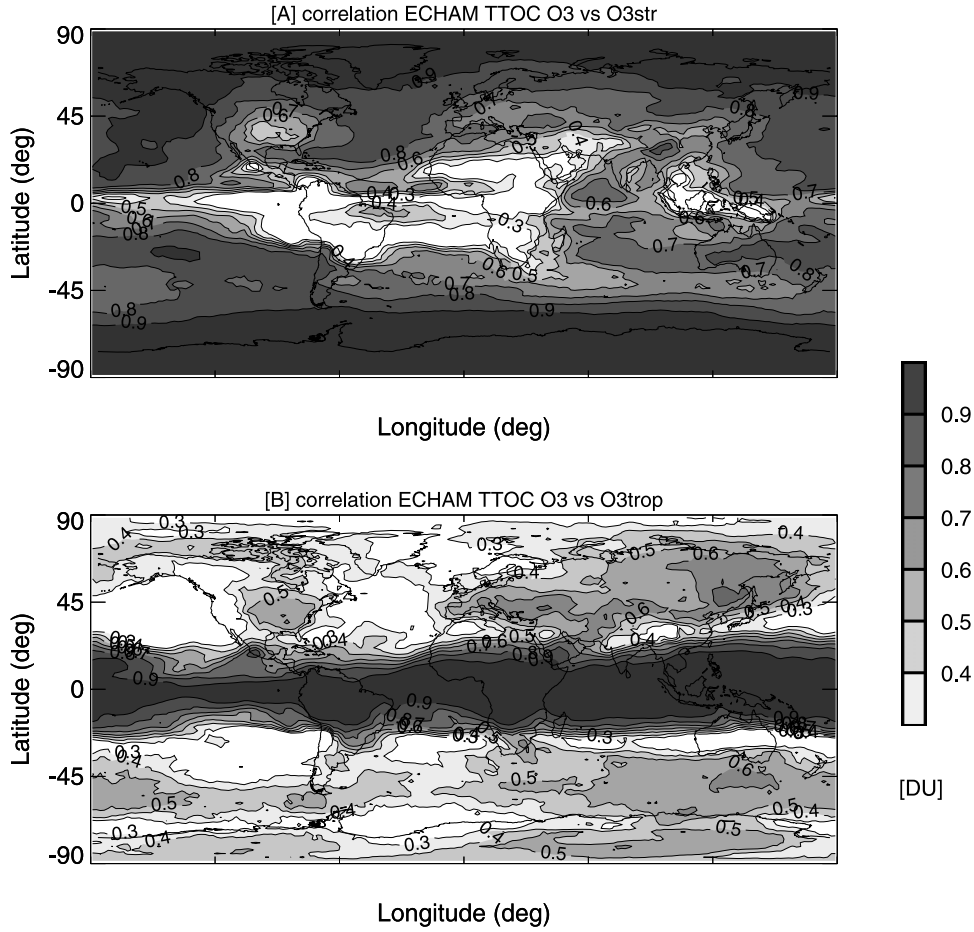

Figure 7. Correlation between the total tropospheric O_3 column and (a) the total tropospheric O_3str column and (b) the total tropospheric O_3trop column. See color version of this figure at back of this issue.

seasonal variations in both contributors. To be able to distinguish between seasonal variations and short-time variations, the seasonality was filtered out using a running mean over 30 days, i.e., subtracting the monthly running mean from the TTOC value. Note that using monthly mean values instead of running mean values yields similar results. Figure 8 shows the correlation between the filtered TTOCs and O_3trop TTOC. Within the tropics a strong correlation between filtered O_3 and O_3trop TTOCs is found. In the Northern Hemisphere, no strong correlation exists between filtered O_3trop and O_3 TTOCs except at high and polar latitudes. By comparing Figure 8 and Figure 7b it can be concluded that the positive correlation between the extratropical Northern Hemisphere O_3 and O_3trop TTOCs must

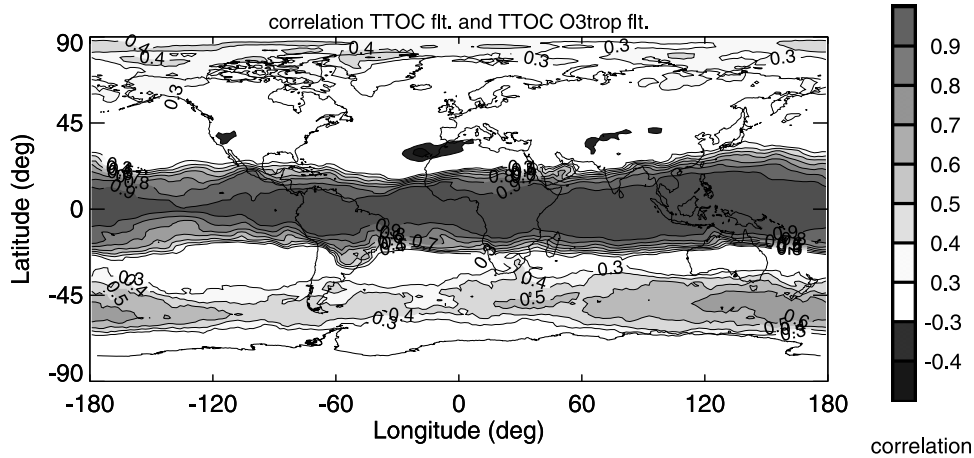

Figure 8. Correlation between filtered O_3 and O_3trop TTOCs. See color version of this figure at back of this issue.

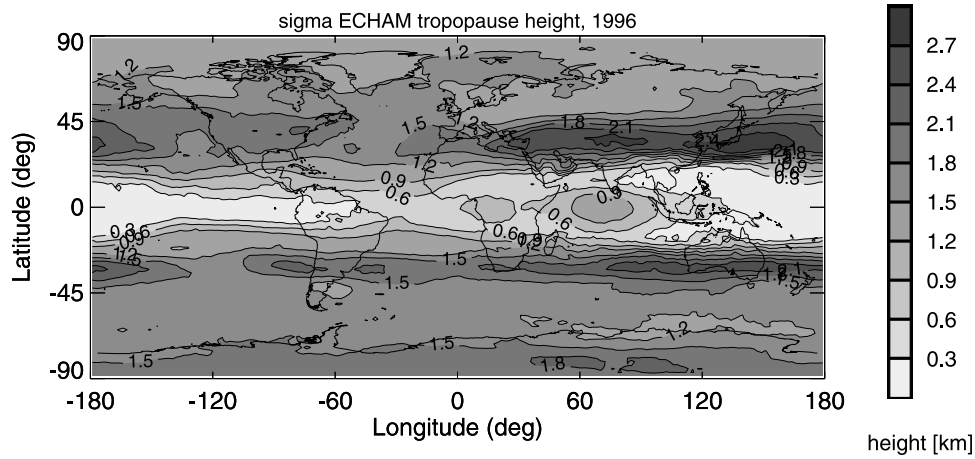

Figure 9. Standard deviation of modeled tropopause heights for 1996 in km. See color version of this figure at back of this issue.

be caused by a strong seasonal cycle. This is in agreement with the fact that the positive correlations occur predominantly over landmasses where most of the O_3 precursors are emitted, which leads to more (less) O_3 production in case of higher (lower) insolation. In the Southern Hemisphere a band with positive correlations between filtered O_3 and O_3trop is found around 45°S, which, as explained before, is related to plumes of O_3trop originating from tropical Africa, South America, and Australia that are transported along the subtropical jet. At the same time a few small areas with a weak negative correlation between filtered O_3 and O_3trop TTOCs can be seen along 30°N (110°W, 0°–70°E), related to the passage of troughs and ridges along the subtropical jet as described in section 4.1. In a trough (high tropospheric, relatively O_3 rich air from midlatitudes advancing south) the contribution of O_3str is larger and that of O_3trop is smaller, whereas in a ridge (lower troposheric, relatively O_3 poor air from tropical latitudes advancing north) the contribution of O_3str is smaller and that of O_3trop is larger.

[31] Figures 5 and 6 showed that (modeled) tropopause height variations play an important role in TTOC variations, especially outside of the tropics. Figure 9 shows the standard deviation of tropopause heights, and Figure 10 shows the correlation between tropopause heights and the TTOC. In the tropics, hardly any correlation can be found between TTOC and tropopause height variations. North of 45°N and south of 45°S a strong correlation exists between tropopause heights and TTOCs for O_3, O_3trop, and O_3str because both O_3trop and O_3str correlate positively with the tropopause height. The differences between the hemispheres are caused by the larger annual variability in Northern Hemispheric sources for tropospheric O_3 (both STE and tropospheric O_3 production). In most of the Southern Hemisphere, variations in tropospheric O_3 due to these two processes are much smaller. However, tropopause height variations in the Northern and Southern Hemisphere are much more similar in magnitude (see Figure 9), and therefore the TTOC variability in the Southern Hemisphere is determined by tropopause height variations more than in the Northern Hemisphere.

6. Requirements for (Satellite) Measurements of TTOCs

[32] In section 1 it was noted that at present several TTOC data sets exist derived from satellite measurements

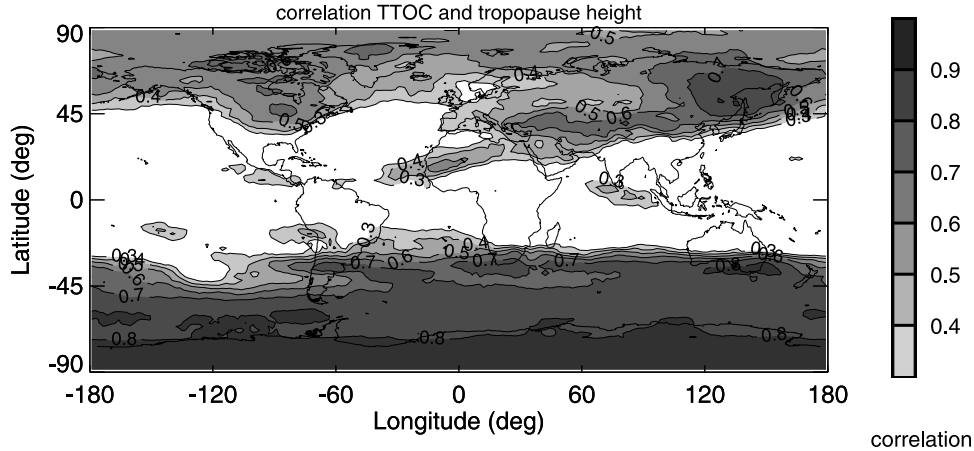

Figure 10. Correlation between modeled tropopause heights and total tropospheric O_3 columns for 1996. See color version of this figure at back of this issue.

Table 3. Standard Deviation of Modeled TTOC Variations During 1996 for the Same Grid Points as Shown in Figures 5 and 6[a]

	TTOC Standard Deviation		TTOC Running Mean Standard Deviation		TTOC Filtered Standard Deviation	
	σ_1	σ_2	Σ_1	σ_2	σ_1	σ_2
66°S	6.6	6.3	3.6	3.6	5.4	5.1
46°S	4.0	4.0	1.1	1.2	3.8	3.7
23°S	3.9	4.7	2.3	2.5	3.0	3.8
1°S	3.9	3.7	2.9	2.7	2.3	2.3
21°N	6.2	6.7	5.4	4.7	2.9	4.5
44°N	9.6	10.1	7.0	7.0	6.3	7.0
66°N	9.1	8.9	5.3	5.5	7.3	6.8
32°N	9.6	8.9	7.6	5.9	5.8	6.3

[a]Shown are standard deviations of the TTOCs, 30-day running mean of the TTOCs and the filtered TTOCs (TTOC minus 30-day running mean TTOC). The σ_1 is the standard deviation of the grid point; the σ_2 is the corresponding mean of all the standard deviations for all different longitudes at the latitude of the grid point.

(error estimates of uncertainties range from 10 to 50% or 5–20 DU due to both random and systematic errors), with most satellite products restricted to tropical latitudes. In our study we investigated whether these uncertainties allow for an analysis of the TTOC variability. The premise here is that the processes that determine most of the TTOC variability should be captured by the measurements. According to the previous sections, variability occurs on seasonal timescales in the tropics, whereas it occurs on seasonal and synoptic timescales outside the tropics.

[33] The accuracies required for measuring these variations can be derived from the typical simulated TTOC variability. Table 3 shows standard deviations (σ) of the modeled TTOCs for both the 30-day running mean and filtered values based on 6-hourly data. In addition, the mean standard deviation of all modeled grid points along the latitude of the selected grid points is shown to illustrate that the selected grid points are representative for that particular latitude. The smallest RMS values occur within the tropics and at Southern Hemisphere midlatitudes, while within the tropics more variability occurs on seasonal timescales. Thus, according to Table 2, monthly mean TTOCs with an error of about 5 DU are sufficient to capture tropical TTOC variability. Note that the results in Table 3 are similar when using daily rather than 6-hourly TTOCs. The variability at NH midlatitudes is larger, and synoptic- and seasonal-scale variations contribute equally, whereas in the SH the short-timescale variations dominate. In order to measure midlatitude TTOC variability one must be able to measure the synoptic-scale variability (see, for example, Figures 5 and 6). The required accuracy for these daily measurements should be at least 10 DU for an individual measurement (1-σ value of TTOC variability in the Northern Hemisphere; Table 1) but preferably 5 DU (1-σ, Southern Hemisphere).

[34] On the basis of current available methods and algorithms, two possibilities exist of achieving the aforementioned accuracies with daily measurements and global coverage. The first option is by performing total column ozone measurements with a high horizontal resolution in combination with stratospheric limb O_3 sounding. The large number of measurements can be averaged to reach the required accuracy, while the limb observations yield the thickness of the stratospheric O_3 column. High spatial resolution also increases the probability of cloud-free observations which are needed for tropospheric measurements. The SCIAMACHY instrument on ENVISAT (launched in 2002) is the first instrument that combines nadir and limb observations for this purpose [*Noël et al.*, 1999]. The footprint of the nadir O_3 measurements is 30×60 km^2. Higher horizontal resolution will be obtained with the Ozone Monitoring Instrument (OMI), which flies on EOS-Aura and has been launched in 2004. OMI will provide global coverage on a daily basis with a pixel size of roughly 15×25 km^2. For a typical model resolution of about 250×250 km^2, 160 observations will be available for determining the TTOC, of which an estimated 15% is cloud-free [*European Space Agency*, 2001]. TTOCs from ESO-Aura will be obtained by combining the limb HIRDLS measurements with the OMI nadir measurements [*Bhartia*, 2002]. The second option is to have geostationary satellite measurements, which perform a number of measurements per day per location, increasing the possibility of cloud-free measurements. An important drawback of geostationary satellites is the lack of limb observations to accurately establish the stratospheric O_3 column.

7. Summary and Conclusions

[35] In this study the role of different processes that determine total tropospheric O_3 column variability was investigated.

[36] Within the tropics TTOC variability is mainly determined by variability in O_3trop. Furthermore, tropopause height variations are small, and most of the variability occurs on seasonal scales associated with the changes from dry to wet seasons and seasonal changes in biomass burning emissions. As a result, monthly mean TTOCs measurements contain most of the information about the important processes causing tropical TTOC variability.

[37] Outside of the tropics the variability of TTOCs is a very complicated interplay between STE, photochemicalO_3 formation, and tropopause height variations. All these processes contribute significantly to the TTOC variability. Furthermore, TTOC variability occurs both on synoptic and seasonal timescales. Variations on synoptic timescales are associated with STE, emission/removal of O_3 precursor and transport associated with synoptical systems, while seasonal variations are associated with stronger STE during local winter and variations in the amount of sunlight which drives photochemistry. It is important to realize that even when the required accuracy is met by the measurements, it still will be difficult to distinguish near-surface O_3 pollution signals. Only additional sources of information will allow determination of the separate contributions to TTOC. Such information could be obtained from either model results (e.g., through data assimilation of remotely sensed O_3) or additional measurements (e.g., NO_x for tropospheric O_3 production and water vapor for STE).

[38] On the basis of this study it can be concluded that in order to be able to measure extratropical TTOC variability, daily measurements with an accuracy of 10 DU or better are required. For tropical TTOC variability, monthly means

with an accuracy of 5 DU or better are sufficient. It should be noted that the accuracies of 5 and 10 DU are not exactly defined values, and that these values will vary with geographical location and season. On the basis of current available methods and algorithms we think that this may be achievable by measuring with a high spatial resolution combining nadir and limb observations (SCIAMACHY or OMI/HIRDLS) or possibly using geostationary measurements. Another possibility would be using a Fourier transform spectrometer to measure in the middle-infrared part of the spectrum (around 10 μm), although it should be noted that daily global coverage can not be achieved. An example of such an instrument is the tropospheric emission spectrometer (TES) on the EOS-Aura platform. *Luo et al.* [2002] and *Worden et al.* [2004] have shown that the expected errors of tropospheric O_3 column measurements by TES are of the order of 10–20% for individual measurements, while in theory up to five tropospheric layers can be measured.

[39] **Acknowledgments.** The authors thank the World Ozone and Ultraviolet radiation Data Centre (WOUDC) for making the ozonesonde data publicly available. The academic computing central in Amsterdam (SARA) is thanked for making their supercomputing facilities available to do the model calculations used for this study. The authors also thank the referees for their valuable remarks and suggestions.

References

Bhartia, P. K. (Ed.) (2002), OMI algorithm theoretical basis document, vol. II, Ozone Monitoring Instrument ozone products, version 2.0, NASA Goddard Space Flight Cent., Greenbelt, Md.

Brasseur, G. P., J. J. Orlando, and G. S. Tyndall (1999), Tropospheric ozone, in *Atmospheric Chemistry and Global Change*, chap. 13, pp. 465–486, Oxford Univ. Press, New York.

Brühl, C., and P. Crutzen (1988), Scenarios of possible changes in atmospheric temperature and ozone concentrations due to man's activities, estimated with a one-dimensional coupled photochemical climate model, *Clim. Dyn.*, *2*, 173–203.

Chandra, S., J. R. Ziemke, W. Min, and W. G. Read (1998), Effects of 1997–1998 El Niño on tropospheric ozone and water vapor, *Geophys. Res. Lett.*, *25*, 3867–3870.

Cristofanelli, P., et al. (2003), Stratosphere-to-troposphere transport: A model and method evaluation, *J. Geophys. Res.*, *108*(D12), 8525, doi:10.1029/2002JD002600.

Creilson, J. K., J. Fishman, and A. E. Wozniak (2003), Intercontinental transport of tropospheric ozone: A study of its seasonal variability across the North Atlantic utilizing tropospheric ozone residuals and its relationship to the North Atlantic Oscillation, *Atmos. Chem. Phys. Discuss.*, *3*, 2053–2066.

de Laat, A. T. J. (2002), On the origin of tropospheric O_3 over the Indian Ocean during the winter monsoon: African biomass burning vs. stratosphere-troposphere exchange, *Atmos. Chem. Phys.*, *2*, 325–341.

European Space Agency (2001), ACECHEM: Atmospheric Composition Explorer for Chemistry and Climate Interaction, *Rep. ESA SP-1257(4)*, Publ. Div., Noordwijk, Netherlands.

Fishman, J., and A. E. Balok (1999), Calculation of daily tropospheric ozone residuals using TOMS and empirically improved SBUV measurements: Application to an ozone pollution episode over the eastern United States, *J. Geophys. Res.*, *104*, 30,319–30,340.

Fishman, J., and V. G. Brackett (1997), The climatological distribution of tropospheric ozone derived from satellite measurements using version 7 Total Ozone Mapping Spectrometer and Stratospheric Aerosol and Gas Experiment data sets, *J. Geophys. Res.*, *102*, 19,275–19,278.

Fishman, J., C. E. Watson, J. C. Larsen, and J. A. Logan (1990), Distribution of tropospheric ozone determined from satellite data, *J. Geophys. Res.*, *95*, 3599–3617.

Fishman, J., A. E. Wozniak, and J. K. Creilson (2003), Global distribution of tropospheric ozone from satellite measurements using the empirically corrected tropospheric ozone residual technique: Identification of the regional aspects of air pollution, *Atmos. Chem. Phys.*, *3*, 1453–1476.

Gery, M., G. Whitten, J. Killus, and M. Dodge (1989), A photochemical kinetics mechanism for urban and regional scale computer modeling, *J. Geophys. Res.*, *94*, 12,925–12,956.

Hoerling, M. P., T. K. Schaack, and A. J. Lenzen (1993), A global analysis of stratospheric tropospheric exchange during northern winter, *Mon. Weather Rev.*, *121*, 162–172.

Holton, J. R., P. H. Haynes, M. E. McIntyre, A. R. Douglass, R. B. Rood, and L. Pfister (1995), Stratosphere-troposphere exchange, *Rev. Geophys.*, *33*, 403–439.

Houweling, S., F. Dentener, and J. Lelieveld (1998), The impact of nonmethane hydrocarbon compounds on tropospheric photochemistry, *J. Geophys. Res.*, *103*, 10,673–10,696.

Hudson, R. D., and A. M. Thompson (1998), Tropical tropospheric ozone from total ozone mapping spectrometer by a modified residual method, *J. Geophys. Res.*, *103*, 22,129–22,145.

Jeuken, A. B. M., P. C. Siegmund, L. C. Heijboer, J. Feichter, and L. Bengtson (1996), On the potential of assimilating meteorological analysis in a climate model for the purpose of model validation, *J. Geophys. Res.*, *101*, 16,939–16,950.

Kentarchos, A. S., and G. J. Roelofs (2003), A model study of stratospheric ozone in the troposphere and its contribution to tropospheric OH production, *J. Geophys. Res.*, *108*(D12), 8517, doi:10.1029/2002JD002598.

Kentarchos, A. S., G. J. Roelofs, and J. Lelieveld (2000), Simulation of extra-tropical synoptic scale stratosphere-troposphere exchange using a coupled chemistry-GCM: Sensitivity to horizontal resolution, *J. Atmos. Sci.*, *57*, 2824–2838.

Kentarchos, A. S., G. J. Roelofs, and J. Lelieveld (2001), Altitude distribution of tropospheric ozone over the Northern Hemisphere during 1996, simulated with a chemistry-general circulation model at two different horizontal resolutions, *J. Geophys. Res.*, *106*(D15), 17,453–17,469.

Kim, J. H., R. D. Hudson, and A. M. Thompson (1998), A new method of deriving time-averaged tropospheric column ozone over the tropics using total ozone mapping spectrometer (TOMS) radiances: Intercomparison and analysis using TRACE A data, *J. Geophys. Res.*, *103*, 24,317–24,330.

Kim, J. H., M. J. Newchurch, and K. Han (2001), Distribution of tropical tropospheric ozone determined by the scan-angle method applied to TOMS measurements, *J. Atmos. Sci.*, *58*, 2699–2708.

Lelieveld, J., and F. Dentener (2000), What controls tropospheric ozone?, *J. Geophys. Res.*, *105*, 3531–3551.

Luo, M., R. Beer, D. J. Jacob, J. A. Logan, and C. D. Rodgers (2002), Simulated observation of tropospheric ozone and CO with the Tropospheric Emission Spectrometer (TES) satellite instrument, *J. Geophys. Res.*, *107*(D15), 4270, doi:10.1029/2001JD000804.

Meloen, J., et al. (2003), Stratosphere-troposphere exchange: A model and method intercomparison, *J. Geophys. Res.*, *108*(D12), 8526, doi:10.1029/2002JD002274.

Newchurch, M. J., X. Liu, J. H. Kim, and P. K. Bhartia (2001), On the accuracy of TOMS retrievals over cloud regions, *J. Geophys. Res.*, *106*, 32,315–32,326.

Newchurch, M. J., D. Sun, J. H. Kim, and X. Liu (2003), Tropical tropospheric ozone derived using clear-cloudy pairs (CCP) of TOMS measurements, *Atmos. Chem. Phys.*, *3*, 683–695.

Noël, S., H. Bovensmann, J. P. Burrows, J. Frerick, K. V. Chance, and A. P. H. Goede (1999), Global atmospheric modeling with SCIAMACHY, *Phys. Chem. Earth*, *24*, 427–434.

Peters, W., M. Krol, F. Dentener, and J. Lelieveld (2001), Identification of an El Niño–Southern Oscillation signal in a multiyear global simulation of tropospheric ozone, *J. Geophys. Res.*, *106*, 10,389–10,402.

Peters, W., M. Krol, F. Dentener, A. M. Thompson, and J. Lelieveld (2002), Chemistry-transport modeling of the satellite observed distribution of tropical tropospheric ozone, *Atmos. Chem. Phys.*, *2*, 103–120.

Pierce, R. B., et al. (2003), Regional Air Quality Modeling System (RAQMS) predictions of the tropospheric ozone budget over east Asia, *J. Geophys. Res.*, *108*(D21), 8825, doi:10.1029/2002JD003176.

Rasch, P. J., and D. Williamson (1990), Computational aspects of moisture transport in global models of the atmosphere, *Q. J. R. Meteorol. Soc.*, *116*, 1071–1090.

Roeckner, E., K. Arpe, L. Bengtsson, M. Christoph, M. Claussen, L. Dümenil, M. Esch, M. Giorgetta, U. Schlese, and U. Schulzweida (1996), The atmospheric general circulation model ECHAM-4: Model description and simulation of present-day climate, *Rep. 218*, Max Planck Inst. for Meteorol., Hamburg, Germany.

Roeckner, E., L. Bengtson, J. Feichter, J. Lelieveld, and H. Rodhe (1999), Transient climate change simulations with an atmosphere-ocean GCM including the tropospheric sulfur cycle, *J. Clim.*, *12*, 3004–3032.

Roelofs, G. J., and J. Lelieveld (1997), Model study of the influence of cross-tropopause O_3 transports on tropospheric O_3 levels, *Tellus, Ser. B*, *49*, 38–55.

Roelofs, G. J., and J. Lelieveld (2000a), Tropospheric ozone simulated with a chemistry-general circulation model: Influence of higher hydrocarbon chemistry, *J. Geophys. Res.*, *105*, 22,697–22,712.

Roelofs, G. J., and J. Lelieveld (2000b), Model analysis of stratosphere-troposphere exchange of ozone and its role in the tropospheric O_3 budget, in *Chemistry and Radiation Changes in the Ozone Layer*, edited by C. Zerefos et al., *NATO Sci. Ser., C*, *557*, 25–43.

Roelofs, G. J., J. Lelieveld, H. Smit, and D. Kley (1997a), Ozone production and transports in the tropical Atlantic region during the biomass burning season, *J. Geophys. Res.*, *102*, 10,637–10,651.

Roelofs, G. J., J. Lelieveld, and R. van Dorland (1997b), A three-dimensional chemistry/general circulation model simulation of anthropogenically derived ozone in the troposphere and its radiative climate forcing, *J. Geophys. Res.*, *102*, 23,389–23,401.

Roelofs, G. J., et al. (2003), Intercomparison of tropospheric ozone models: Ozone transport in a complex tropopause folding event, *J. Geophys. Res.*, *108*(D12), 8529, doi:10.1029/2003JD003462.

Thompson, A. M., and R. D. Hudson (1999), Tropical tropospheric ozone (TTO) maps from Nimbus 7 and Earth Prober TOMS by the modified-residual method: Evaluation with sondes, ENSO signals, and trends from Atlantic regional time series, *J. Geophys. Res.*, *104*, 26,961–26,975.

Thompson, A. M., K. E. Pickering, D. P. McNamara, M. R. Schoeberl, R. D. Hudson, J. H. Kim, E. V. Browell, V. W. J. H. Kirchhoff, and D. Nganga (1996), Where did tropospheric zone over southern Africa and the tropical Atlantic come from in October 1992? Insights from TOMS, GTE TRACE A, and SAFARI 1992, *J. Geophys. Res.*, *101*, 24,251–24,278.

Thompson, A. M., J. C. Witte, R. D. Hudson, H. Guo, J. R. Herman, and M. Fuijiwara (2001), Tropical tropospheric ozone and biomass burning, *Science*, *291*, 2128–2132.

Valks, P. J. M., R. B. A. Koelemeijer, M. van Weele, P. van Velthoven, J. P. F. Fortuin, and H. Kelder (2003), Variability in tropical tropospheric ozone: Analysis with Global Ozone Monitoring Experiment observations and a global model, *J. Geophys. Res.*, *108*(D11), 4328, doi:10.1029/2002JD002894.

von Kuhlman, R. (2001), Tropospheric photochemistry of ozone, its precursors and the hydroxyl radical: A 3-D modeling study considering non-methane hydrocarbons, Ph.D. thesis, Univ. of Mainz, Mainz, Germany.

Wernli, H., and M. Bourqui (2002), A Lagrangian "1-year climatology" of (deep) cross-tropopause exchange in the extratropical Northern Hemisphere, *J. Geophys. Res.*, *107*(D2), 4021, doi:10.1029/2001JD000812.

Worden, J., S. S. Kulawik, M. W. Shephard, S. A. Clough, H. Worden, K. Bowman, and A. Goldman (2004), Predicted errors of tropospheric emission spectrometer nadir retrievals from spectral window selection, *J. Geophys. Res.*, *109*, D09308, doi:10.1029/2004JD004522.

Ziemke, J. R., and S. Chandra (1999), Seasonal and interannual variabilities in tropical tropospheric ozone, *J. Geophys. Res.*, *104*, 21,425–21,442.

Ziemke, J. R., A. M. Thompson, and D. P. McNamara (1996), Zonal asymmetries in Southern Hemisphere column ozone: Implications of biomass burning, *J. Geophys. Res.*, *101*, 14,421–14,427.

Ziemke, J. R., S. Chandra, and P. K. Bhartia (1998), Two new methods for deriving tropospheric column ozone from TOMS measurements: Assimilated UARS MLS/HALOE and convective-cloud differential techniques, *J. Geophys. Res.*, *103*, 22,115–22,127.

I. Aben and A. T. J. de Laat, National Institute for Space Research (SRON), Utrecht, Netherlands. (a.t.j.de.laat@sron.nl)

G. J. Roelofs, Institute for Marine and Atmospheric Research (IMAU), Utrecht University, Utrecht, Netherlands.

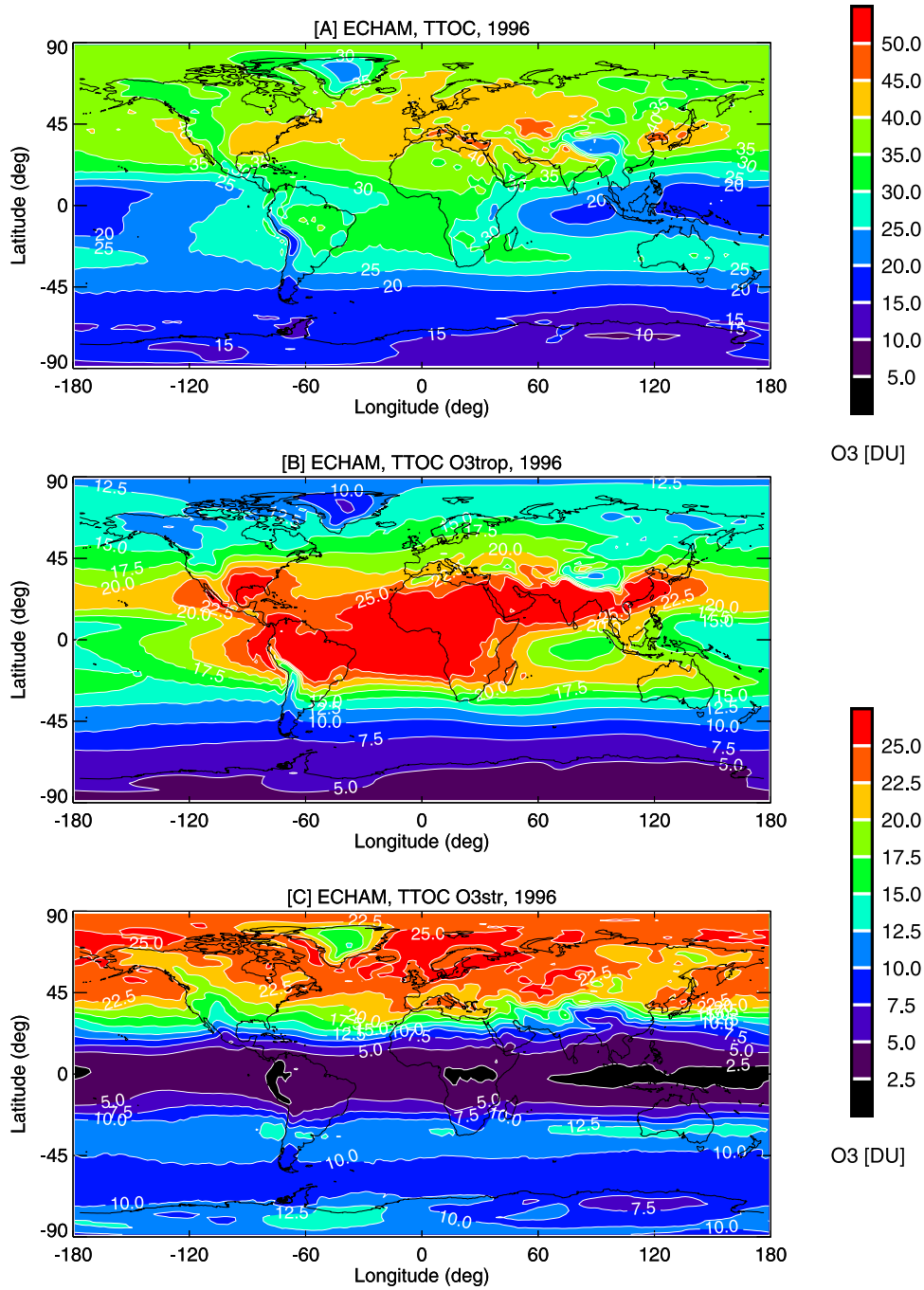

Figure 2. Annual (1996) average total tropospheric O_3 column density (Dobson units, or DU) for (a) O_3, (b) tropospheric O_3 production, and (c) O_3 of stratospheric origin.

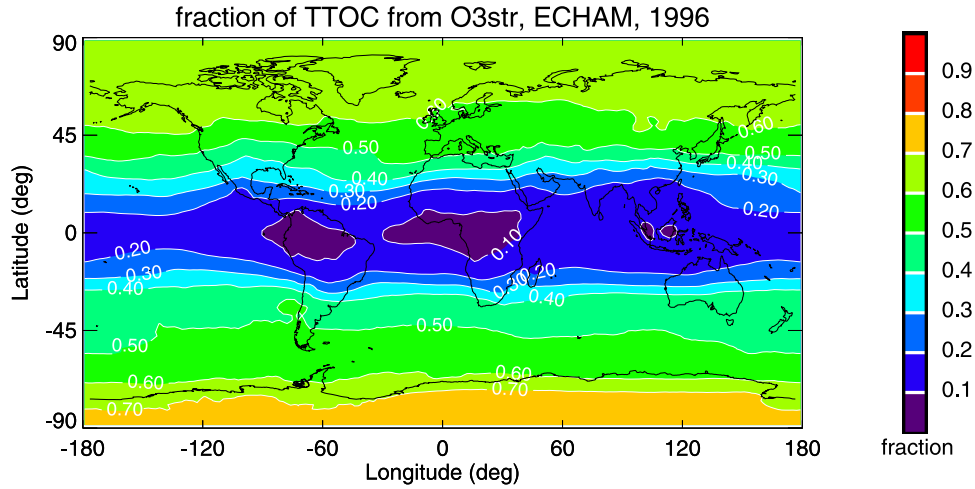

Figure 3. Annual (1996) average fraction of ECHAM modeled total tropospheric O_3 columns attributed to O_3 of stratospheric origin. The residual of this value (that is one minus this values) denotes the contribution of O_3 of tropospheric origin.

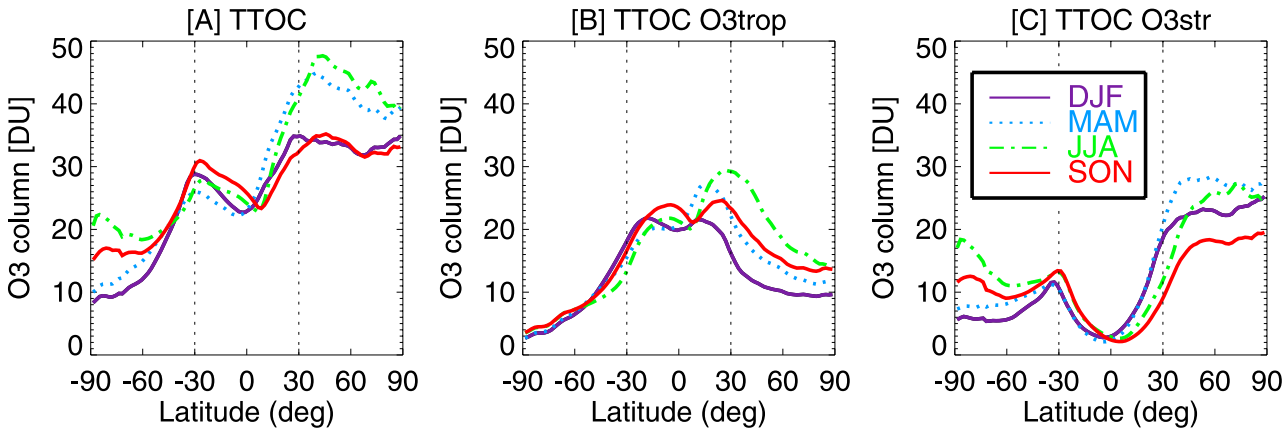

Figure 4. The zonal averaged total tropospheric O_3 column (DU) as a function of season (purple solid curve, DJF; dotted blue curve, MAM; dash-dotted green curve, JJA; dash-dotted red curve, SON). Indicated are (a) the total tropospheric O_3 column, (b) the O_3trop, and (c) O_3str contribution to the total tropospheric O_3 column.

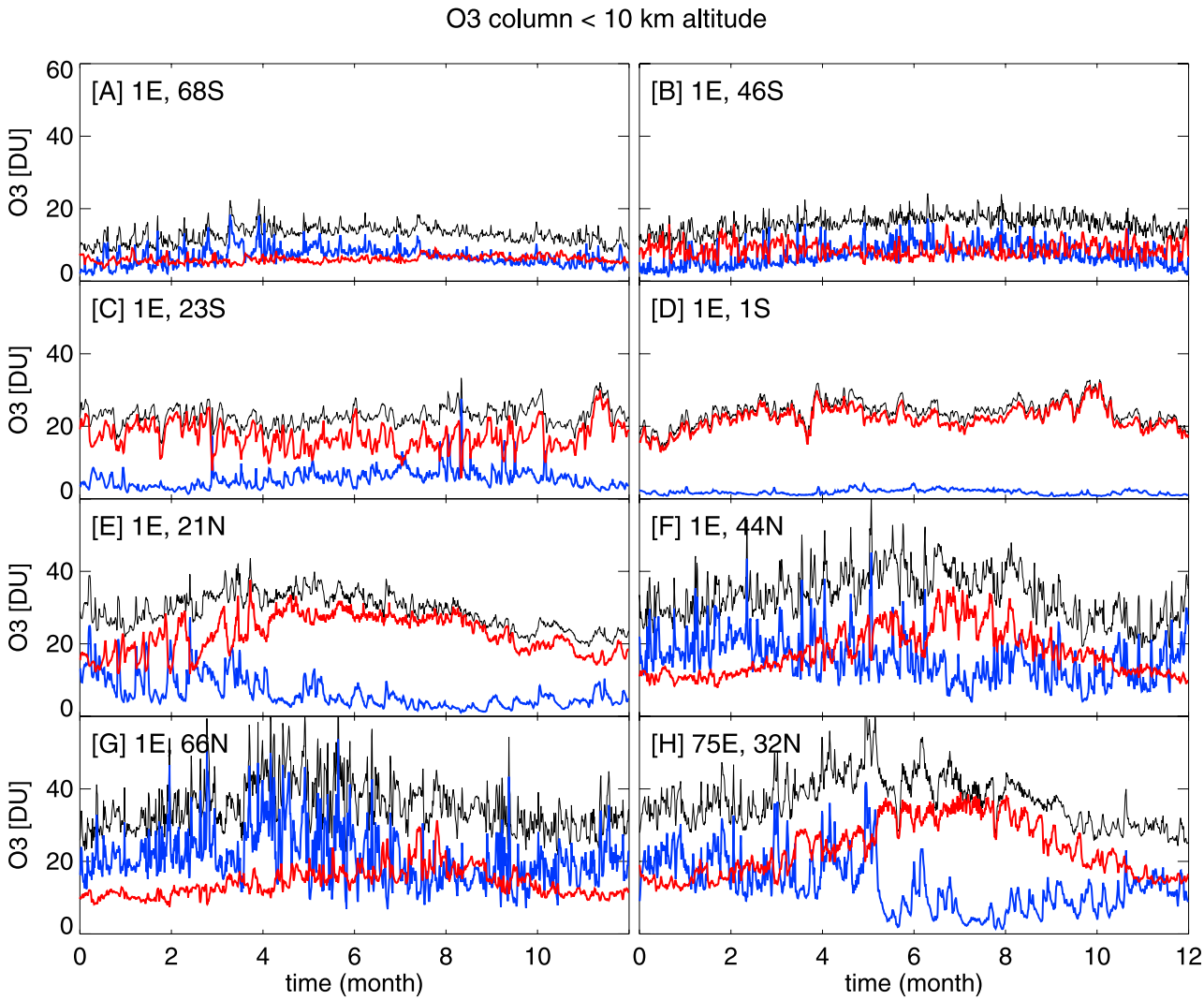

Figure 5. Total O_3 columns (black curve) between the surface and 10-km altitude and the respective O_3trop (red curve) and O_3str (blue curve) partitioning at seven latitudes along 1°E from (a–g) 68°S to 66°N and (h) at 32°N–75°E for the year 1996. The total O_3 column between the surface and 10-km altitude is not affected by tropopause height variations.

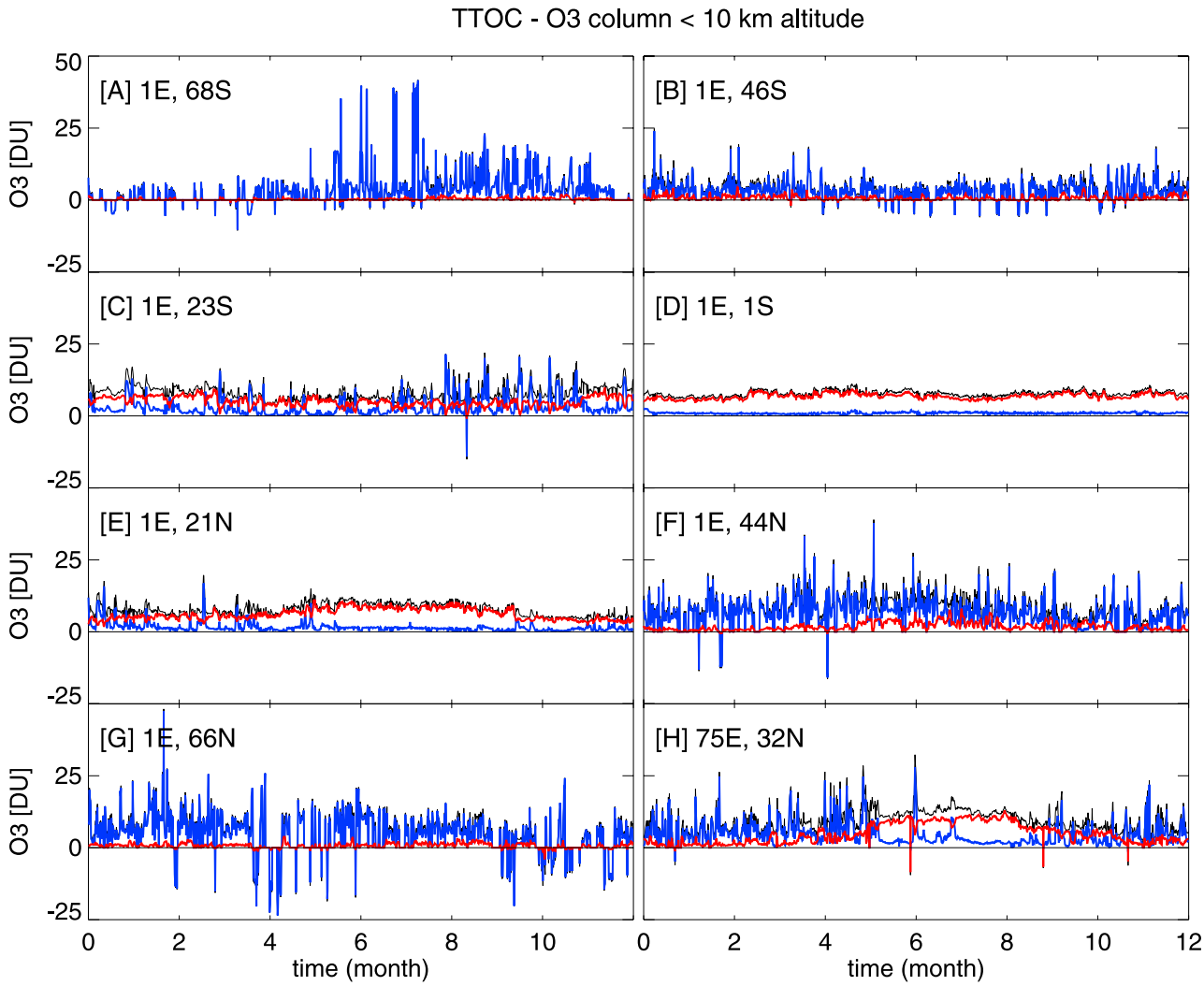

Figure 6. Same as Figure 5 but for the difference between the total tropospheric O_3 column density and the O_3 column between the surface and 10-km altitude.

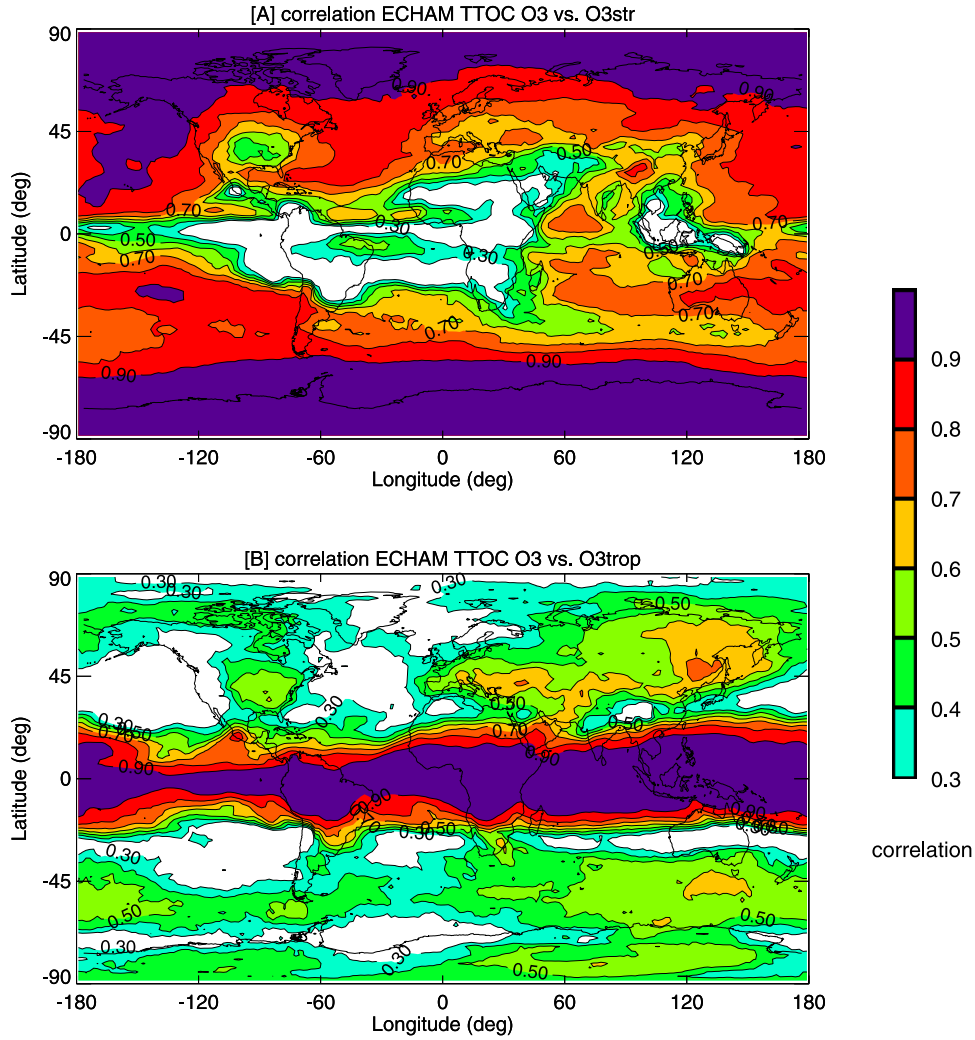

Figure 7. Correlation between the total tropospheric O_3 column and (a) the total tropospheric O_3str column and (b) the total tropospheric O_3trop column.

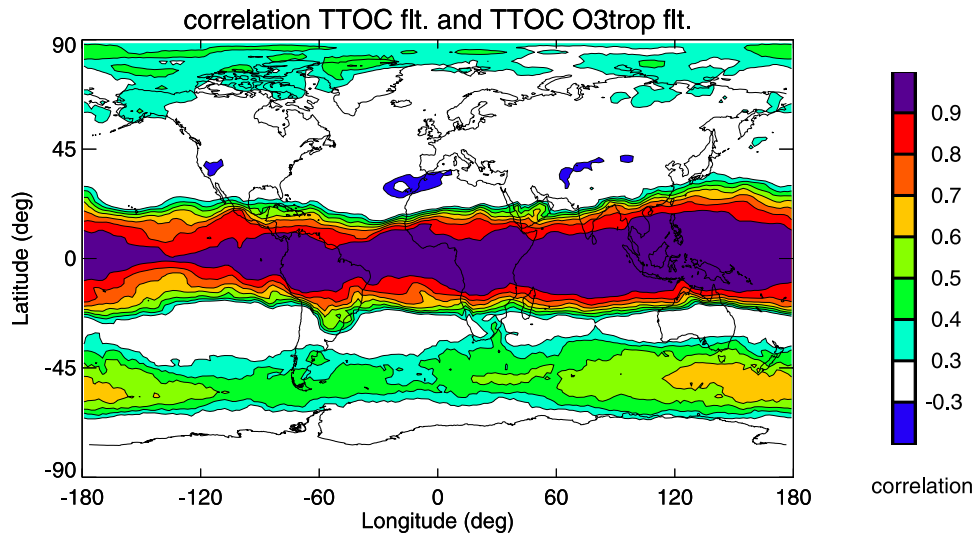

Figure 8. Correlation between filtered O_3 and O_3trop TTOCs.

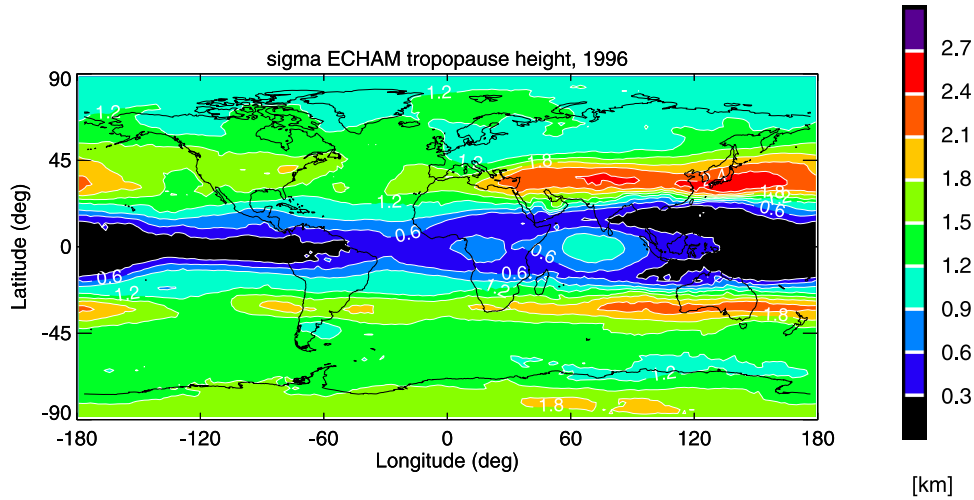

Figure 9. Standard deviation of modeled tropopause heights for 1996 in km.

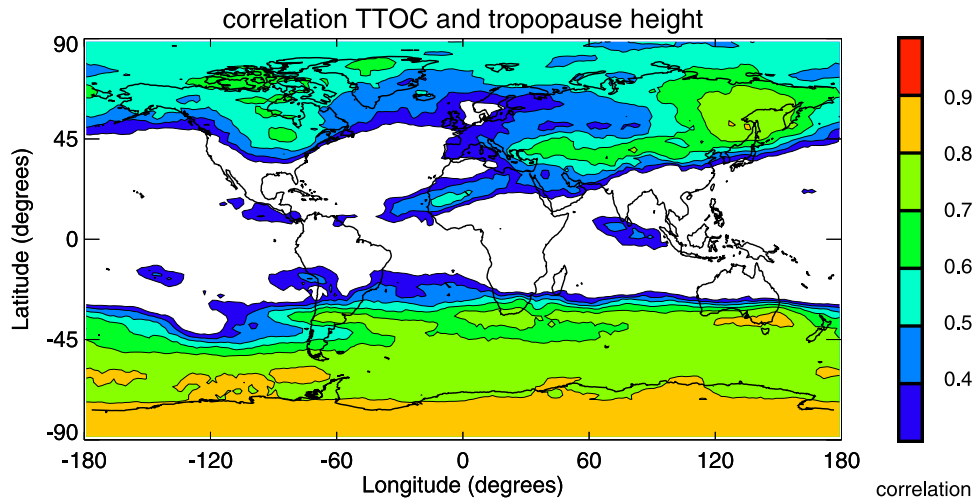

Figure 10. Correlation between modeled tropopause heights and total tropospheric O_3 columns for 1996.